

1 **SARS-CoV-2 Nsp14 activates NF- κ B signaling and induces IL-8 upregulation**

2

3 **Authors**

4 Taiwei Li¹, Adam D. Kenney², Helu Liu³, Guillaume N. Fiches¹, Dawei Zhou¹, Ayan Biswas⁴, Jianwen
5 Que³, Netty Santoso¹, Jacob S. Yount², and Jian Zhu^{1,2, *}

6

7 **Affiliations**

8 1. Department of Pathology, The Ohio State University Wexner Medical Center, Columbus, OH 43210,
9 USA

10 2. Department of Microbial Infection and Immunity, The Ohio State University Wexner Medical Center,
11 Columbus, OH 43210, USA

12 3. Department of Medicine, Columbia University Medical Center, New York, NY 10032, USA

13 4. Department of Genetics, The University of Alabama at Birmingham, Birmingham, AL 35233, USA

14

15 * To whom correspondence should be addressed: Jian Zhu (Jian.Zhu@osumc.edu)

16

17 **Keywords:** SARS-CoV-2, NF- κ B, IL-8, IMPDH2, ribavirin, mycophenolic acid

18

19

20

21

22

23

24 **Summary**

25 Severe acute respiratory syndrome coronavirus 2 (SARS-CoV-2) infection leads to NF- κ B activation
26 and induction of pro-inflammatory cytokines, though the underlying mechanism for this activation is not
27 fully understood. Our results reveal that the SARS-CoV-2 Nsp14 protein contributes to the viral activation
28 of NF- κ B signaling. Nsp14 caused the nuclear translocation of NF- κ B p65. Nsp14 induced the
29 upregulation of IL-6 and IL-8, which also occurred in SARS-CoV-2 infected cells. IL-8 upregulation was
30 further confirmed in lung tissue samples from COVID-19 patients. A previous proteomic screen identified
31 the putative interaction of Nsp14 with host Inosine-5'-monophosphate dehydrogenase 2 (IMPDH2)
32 protein, which is known to regulate NF- κ B signaling. We confirmed the Nsp14-IMPDH2 protein
33 interaction and found that IMPDH2 knockdown or chemical inhibition using ribavirin (RIB) and
34 mycophenolic acid (MPA) abolishes Nsp14-mediated NF- κ B activation and cytokine induction.
35 Furthermore, IMPDH2 inhibitors (RIB, MPA) efficiently blocked SARS-CoV-2 infection, indicating that
36 IMPDH2, and possibly NF- κ B signaling, is beneficial to viral replication. Overall, our results identify a
37 novel role of SARS-CoV-2 Nsp14 in causing the activation of NF- κ B.

38

39 **Introduction**

40 SARS-CoV-2 is a beta-coronavirus that causes the current, severe COVID-19 pandemic globally. The
41 viral genome of SARS-CoV-2 is a ~30 kb polycistronic, positive-strand RNA that encodes multiple
42 structural and nonstructural proteins (1, 2). SARS-CoV-2 nonstructural proteins (Nsp1-16) play
43 diversified roles in supporting viral RNA/protein synthesis and virion assembly, including manipulating
44 host gene expression and host antiviral responses (3, 4). It has been recently reported that SARS-CoV-2
45 infection suppresses type I interferon (IFN) signaling (5, 6), while it induces the activation of NF- κ B
46 signaling that plays a central role in the production of pro-inflammatory cytokines, including interleukin

47 (IL)- 6 and IL-8 (5, 7, 8). In certain cases, massive inflammatory responses occur due to hyper-activation
48 of the immune system, resulting in a widespread and uncontrolled cytokine storm, leading to acute
49 respiratory distress syndrome (ARDS), life-threatening lung damage, and increased mortality of COVID-
50 19 patients. However, the underlying mechanism of how SARS-CoV-2 infection contributes to NF- κ B-
51 mediated inflammatory responses that are expected to determine the outcome of SARS-CoV-2 viral
52 replication and pathogenesis is still largely uncharacterized.

53 Here we focused on characterizing the regulatory functions of SARS-CoV-2 Nsp14 that are required
54 for efficient viral replication. Nsp14 is a conserved, multifunctional viral factor participating in
55 synthesizing and modifying coronaviral sub-genomic (sg) RNAs (9). Nsp14 possesses a 3' to 5'
56 exonuclease activity that excises mismatched base pairs during viral RNA replication (10-12), providing
57 a proofreading function that increases the fidelity of viral RNA synthesis (13, 14). Nsp14 also possesses
58 RNA methyltransferase activity required for guanine-N7 methylation (15). Nsp14-mediated guanine-N7
59 methylation cooperates with 2'-O RNA methylation mainly catalyzed by Nsp10/16, leading to 5'-capping
60 of newly synthesized sgRNAs (16, 17), which not only prevents degradation by host RNA 5' exonucleases
61 and recognition by host foreign RNA sensors, such as RIG-I (18), but also increases translation efficiently
62 of host ribosomes to synthesize viral proteins (19, 20). Nsp14 has also been reported to reduce the
63 accumulation of viral double-stranded (ds) RNAs and thus dampen the pathogen-associated molecular
64 pattern (PAMP) mediated antiviral response (21). In addition, Nsp14 is known to facilitate recombination
65 between different viral RNAs to generate new strains (22). Compared to these well-studied viral functions
66 of Nsp14, its regulation of host cellular events is much less investigated. An earlier large-scale proteomic
67 analysis reporting candidate interacting partners for all of the SARS-CoV-2 open reading frames (ORFs)
68 indicated that the host inosine-5'-monophosphate dehydrogenase 2 (IMPDH2) protein is one binding
69 partner of SARS-CoV-2 Nsp14 protein (23). Interestingly, IMPDH2 has been identified to play a role in

70 regulating NF- κ B signaling (24). Our new results showed that SARS-CoV-2 Nsp14 activates NF- κ B
71 signaling and induces IL-8 upregulation, which indeed requires the interaction of Nsp14 with IMPDH2.

72

73 **Results**

74 **SARS-CoV-2 Nsp14 causes activation of NF- κ B.**

75 We initially investigated the effect of SARS-CoV-2 Nsp14 along with Nsp10 and Nsp16 on certain
76 immune signaling pathways. The pcDNA-V5-FLAG-Nsp14/10/16 vectors were individually transfected
77 in HEK293T, and the expression of the individual proteins was confirmed (**Fig S1A**). We then utilized
78 these expression vectors for interferon-sensitive response element (ISRE) and NF- κ B luciferase reporter
79 assays (**Fig S1B and C**). Nsp14 mildly increased ISRE activity at the basal level but caused its decrease
80 in IFN- α -treated HEK293T cells, while Nsp10 and Nsp16 mildly decreased ISRE activity at both
81 conditions, which is consistent with earlier findings (3, 4). On the contrary, only Nsp14 significantly
82 increased NF- κ B activity in both untreated and TNF- α -treated HEK293T cells. TNF- α did not affect the
83 expression of transfected Nsp14 in HEK293T cells (**Fig 1A**) but induced a drastic increase of NF- κ B
84 activity that was further enhanced by Nsp14 (**Fig 1B**). Thus, we further investigated Nsp14-induced
85 activation of NF- κ B signaling. The impact of Nsp14 on nuclear localization of NF- κ B p65 was determined
86 in HEK293T cells transfected with Nsp14. Indeed, Nsp14 expression led to the significant increase of
87 nuclear but not total p65 protein (**Fig 1C, D and Fig S2**). These results confirmed that SARS-CoV-2
88 Nsp14 activates NF- κ B signaling.

89 **SARS-CoV-2 Nsp14 induces upregulation of IL-8.**

90 NF- κ B plays a critical role in regulating pro-inflammatory gene expression. Since we showed that
91 Nsp14 causes NF- κ B activation, we further determined whether Nsp14 induces the expression of several
92 interleukins (IL-4, 6, 8). IL-6 and IL-8 are defined gene targets of NF- κ B (25-27). In HEK293T cells

93 transfected with pcDNA-V5-FLAG-Nsp14, IL-6 and IL-8 were consistently and significantly upregulated
94 with or without TNF- α (**Fig 2A**). Results were similar in Nsp14-transfected A549 cells, although it was
95 significant only in experiments without TNF- α (**Fig 2B**). As a control, we confirmed that TNF- α does not
96 affect the expression of transfected Nsp14 in A549 cells (**Fig S3**). In contrast to IL-6 and IL-8, IL-4 was
97 not induced by Nsp14 in HEK293T nor A549 cells.

98 We next confirmed whether infection of cells with SARS-CoV-2 also induces upregulation of IL-6
99 and IL-8. HEK293T-ACE2 cells were infected with the SARS-CoV-2 viral strain USA-WA1/2020 (28).
100 Expression of viral genes, Nsp14 and nucleocapsid [N], was readily detected (**Fig 2C**). The SARS-CoV-
101 2 infection also led to the upregulation of IL-6 and IL-8, but not IL-4 (**Fig 2D**). We employed
102 immunofluorescence staining assays to determine whether IL-8 upregulation occurs in lung tissue
103 samples dissected from deceased COVID-19 patients. The results showed that IL-8 expression is
104 consistently higher in COVID-19 patients (**Fig 2E**) compared to un-infected cases (**Fig 2F**). IL-6 induction
105 in the lung of COVID-19 patients has already been reported elsewhere (29, 30). We primarily focused on
106 IL-8 as the representative target gene of NF- κ B for further analysis since its induction by Nsp14 is overall
107 more robust than IL-6.

108 **IMPDH2 binds to Nsp14 and contributes to Nsp14 induction of IL-8.**

109 We first confirmed the putative protein interaction of Nsp14 with IMPDH2 (23) by protein co-
110 immunoprecipitation (co-IP) assays in HEK293T cells co-transfected with the pLEX-V5-IMPDH2 and
111 pEZY-FLAG-Nsp14 vectors (**Fig 3A**). As the next step, we determined whether endogenous IMPDH2 is
112 required for IL-8 induction by Nsp14. IMPDH2-targeting or non-targeting (NT) siRNAs were transfected
113 in HEK293T cells, and efficient knockdown of endogenous IMPDH2 was confirmed (**Fig 3B**).
114 Remarkably, IMPDH2 knockdown abolished the IL-8 induction by Nsp14 in HEK293T cells without or

115 with TNF- α (**Fig 3C**). However, overexpression of IMPDH2 had no significant effect on NF- κ B activation
116 by Nsp14 in HEK293T cells with or without TNF- α (**Fig S4**).

117 **IMPDH2 inhibition blocks Nsp14-mediated NF- κ B activation and IL-8 induction.**

118 Since IMPDH2 is required for IL-8 induction by Nsp14, we expected that its inhibition would reduce
119 Nsp14-mediated NF- κ B activation and IL-8 induction. We tested two reported IMPDH2 inhibitors,
120 ribavirin (RIB) and mycophenolic acid (MPA) (23, 31). RIB is a synthetic nucleoside that occupies the
121 IMPDH2 catalytic site to inhibit IMP conversion to xanthosine 5'-phosphate (XMP) during the guanine
122 nucleotide (GTP) biosynthesis (31-33). MPA shares similar features with the IMPDH2 cofactor,
123 nicotinamide adenine dinucleotide (NAD⁺). MPA stacks and traps the XMP intermediate at the catalytic
124 site to inhibit IMPDH2 enzyme activity (31, 34). We confirmed that NF- κ B activation by Nsp14
125 significantly decreases in HEK293T cells treated with RIB (**Fig 4A**) or MPA (**Fig 4B**) at multiple doses
126 in the absence or presence of TNF- α using the NF- κ B luciferase reporter assays. Likewise, treatment of
127 HEK293T cells with RIB (**Fig 4C**) or MPA (**Fig 4D**) also caused the reduction of IL-8 induction by Nsp14.
128 We next tested whether IMPDH2 inhibitors (RIB, MPA) also repress SARS-CoV-2 infection *in vitro*,
129 considering that virus-mediated NF- κ B activation would likely benefit its replication (35-38). Indeed, we
130 showed that the infection rate of SARS-CoV-2 decreases in both A549-ACE2 and HEK293T-ACE2 cells
131 treated with RIB or MPA through quantification of cells expressing N protein by immunofluorescence
132 staining assays (**Fig 4E-F, S5A-B**) or sgRNA level by RT-qPCR (**Fig 4G, S5C**). Consistently, we also
133 identified that treatment of RIB or MPA leads to a significant reduction of IL-8 expression (**Fig 4H**).

134

135 **Discussion**

136 Besides the well-known viral functions of SARS-CoV-2 Nsp14 to control modification and replication
137 of viral RNA genomes, earlier studies illustrated that Nsp14 suppresses Type 1 IFN signaling and nuclear

138 translocation of IRF3 to facilitate viral invasion of the host's antiviral immune response (3, 4). Our results
139 showed that Nsp14, which is expressed at the early stage of primary infection (7), also affects other cell
140 signaling pathways, such as NF- κ B signaling (**Fig 1**), likely to support viral replication. Activation of NF-
141 κ B may further trigger the production of downstream pro-inflammatory cytokines to initiate the cytokine
142 storm and contribute to ARDS. In this study, we identified that Nsp14 increases nuclear translocation of
143 p65 and induces expression of NF- κ B's downstream cytokines, such as IL-6 and IL-8, which have also
144 been detected in lung tissues of COVID-19 patients (5, 29) and animal models of SARS-CoV-2 infection
145 (7). These cytokines are reported to play a critical role in regulating the recruitment and infiltration of
146 immune cells (macrophages, neutrophils) during viral infection (39, 40). Infiltrating immune cells may
147 further escalate inflammatory responses leading to lung damage. Indeed, we showed that IL-8 expression
148 is much higher in lung tissue samples of COVID-19 patients than in uninfected controls (**Fig 2E, F**).

149 Another key finding is that IMPDH2 is a host mediator of Nsp14 involved in NF- κ B activation,
150 verified by both genetic knockdown (**Fig 3**) and chemical inhibition (**Fig 4**). We confirmed the protein
151 interaction of Nsp14 with IMPDH2, which was initially reported in earlier proteomic studies (23, 29).
152 Previous results also suggested that IMPDH2 benefits budding of Junin mammarenavirus (JUNV),
153 propagation of lymphocytic choriomeningitis virus (LCMV) (41), and replication of human norovirus
154 (HuNV) (42). IMPDH2 inhibitors have been used for treating hepatitis C virus (HCV) (31, 43). Our results
155 suggested that IMPDH2 likely supports the SARS-CoV-2 infection and Nsp14-mediated NF- κ B
156 activation as well. IMPDH2 is a protein target of certain immunosuppressive drugs used for organ
157 transplantation and allograft rejection (34, 44, 45), and it has been reported to regulate NF- κ B signaling
158 (24, 46). Nsp14 may hijack IMPDH2 for NF- κ B activation (24), contributing to abnormal inflammatory
159 responses. In terms of possible molecular mechanisms, since IMPDH2 participates in regulating the host
160 nucleotide metabolism (47, 48), it may further modulate cellular stress response and downstream NF- κ B

161 activation (48-50). Nsp14 may manipulate IMPDH2 to increase the phosphorylation of IKK β and I κ B α to
162 promote nuclear translocation and phosphorylation of p65 (24). In addition, we also noticed that Nsp14
163 partially localizes in the nuclei of cells (**Fig 1C, D**), similar to findings from other groups (51, 52). Thus,
164 Nsp14 may associate with and modify the host cellular RNAs via its exonuclease and methyltransferase
165 activities. Nsp14 may also affect the transcriptional activity of nuclear p65 and the expression of its gene
166 targets. Future studies will be needed for further understanding how Nsp14 and IMPDH2 cooperate to
167 activate NF- κ B.

168 Our study has the translational significance since we showed that IMPDH2 inhibitors, RIB and MPA,
169 effectively reduce viral replication of SARS-CoV-2 and expression of NF- κ B's downstream cytokines
170 (IL-6 and IL-8) induced by SARS-CoV-2 (**Fig 4E-H**). It has been reported that IL-8 increases the
171 replication of human immunodeficiency virus-1 (HIV-1), HCV, and cytomegalovirus (CMV) (53-56).
172 SARS-CoV-2 Nsp14 induces the NF- κ B signaling and downstream cytokines, which may support the host
173 cell proliferation and survival, or prevent cell apoptosis, thus benefiting viral replication (38, 57). RIB
174 and MPA are both FDA-approved drugs for treating HCV infection and transplant organ rejection,
175 respectively. Our findings are supported by recent results showcasing the therapeutic potential of RIB and
176 MPA for treating COVID-19 and SARS-CoV-2 infection. The combination of RIB with IFN β -1b and
177 Lopinavir–Ritonavir therapy is currently in clinical trials for treating SARS-CoV-2 infection (58), which
178 has been shown to significantly alleviate the COVID-19 symptoms and suppress IL-6 levels in serum. In
179 another preclinical study, MPA was reported to inhibit SARS-CoV-2 replication (59) and viral entry (60).
180 Our study delineated a potentially new mode of action (MOA) for these IMPDH2 inhibitors, which may
181 disrupt the Nsp14-IMPDH2 axis that plays a crucial role in regulating activation of NF- κ B signaling and
182 induction of its downstream cytokines (**Fig 5**).

183

184 **Material and Methods**

185 **Cell culture**

186 HEK293T cells (Cat. # CRL-3216, ATCC) were cultured in Dulbecco's modified Eagle's medium
187 (DMEM, Cat # D5796, Sigma). A549 cells (Cat. # CCL-185, ATCC) were cultured in F12K medium (Cat.
188 # 21127030, Gibco™). Vero E6 cells (Cat. # CRL-1586, ATCC) were cultured in DMEM. HEK293T
189 cells stably expressing ACE2-GFP were previously described (28). A549-ACE2 cells were obtained
190 through BEI Resources, NIH, NIAID (Cat # NR53821). Cell culture medium contained 10% fetal bovine
191 serum (FBS, Cat. # 10437028, Thermo Fisher), penicillin (100 U/ml) /streptomycin (100 µg/ml) (Cat. #
192 MT30002CI, Corning).

193 **Compounds and antibodies**

194 Recombinant human TNF- α (Cat. # 554618) was purchased from BD. Biosciences. Ribavirin (RIB,
195 Cat. # R0077) was purchased from Tokyo Chemical Industry (TCI). Mycophenolic acid (MPA, Cat. #
196 M3546) was purchased from Sigma-Aldrich. Anti-V5 (Cat. # R960-25), HRP-conjugated anti-V5, and
197 goat HRP-conjugated anti-mouse IgG (H+L) secondary antibody (Cat. # 31430) were purchased from
198 Thermo Fisher Scientific. Anti-GAPDH antibody (Cat. # sc-32233) was purchased from Santa Cruz
199 Biotechnology. Anti-FLAG (Cat. # 2368) antibody, anti-H3 antibody (Cat. # 9715S), and goat HRP-
200 conjugated anti-rabbit IgG antibody (Cat. # 7074) were purchased from Cell Signaling Technology. Anti-
201 IL8 antibody (Cat. # 554717) was purchased from BD. Biosciences.

202 **Plasmids**

203 pLEX-IMP2H2-V5 vector was picked from the MISSION TRC3 human LentiORF library from
204 Sigma-Aldrich. The pcDNA-FLAG-V5-Nsp10/14/16 vectors were constructed from pDONR223 SARS-
205 CoV-2 Nsp10 (Cat. # 141264, Addgene), Nsp14 (Cat. # 141267, Addgene), and Nsp16 (Cat. # 141269,
206 Addgene) vectors to the pcDNA3.1-3xFLAG-V5-ccdB (Cat. # 87064, Addgene) destination vector using

207 Gateway™ LR Clonase™ II Enzyme Mix (Cat. # 11791020, Invitrogen). pEZY-FLAG-Nsp14 vector was
208 constructed from pDONR223 SARS-CoV-2 Nsp14 vector to the pEZY-FLAG (Cat # 18700, Addgene)
209 destined vector. The pLEX-FLAG-V5 vector was constructed by cloning the FLAG sequence to the
210 pLEX-307 (Cat # 41392, Addgene) vector. The pNF-κB-luciferase vector (PRDII4–luc in the pGL3 vector)
211 was the gift from Dr. Jacob Yount's lab (61). The pIRES-luciferase vector (Cat. # 219092) was acquired
212 from Agilent Technologies. The pRL-TK Renilla Luciferase vector (Cat. # AF025846) was purchased
213 from Promega.

214 **Transient transfection**

215 For Nsp14 overexpression, we performed the transient transfection in HEK293T or A549 cells using
216 TurboFect transfection reagents (Cat. # R0531, Thermo Scientific). Briefly, cells were seeded and
217 incubated with the mixture of plasmids with Turbofect (2 μg plasmid DNA / $\sim 3 \times 10^5$ cells) for 24 h. The
218 medium was changed, followed by treatment of TNF-α or compounds. For IMPDH2 knockdown, 50 nM
219 siRNA (IMPDH2 assay ID: s7417, sense: 5'-CCAAGAAAUCACUCUUt-3'; anti-sense: 5'-
220 UUAAGAGUGAUUUUCUUGGtc-3', Ambion by Life technologies; non-targeting control: Silencer™
221 Negative Control No. 4 siRNA, si NT, Cat. # AM4641, Invitrogen) was reversely transfected in HEK293T
222 cells using Lipofectamine™ RNAiMAX Transfection Reagent (Cat. # 13778030, Invitrogen). Cells were
223 kept in culture for 48h and subjected to qPCR analysis for measurement of gene expression.

224 **Protein immunoblotting**

225 Protein immunoblotting was performed following our previously published protocols (62, 63). Briefly,
226 cells were harvested, washed by PBS, and pelleted. Cell pellets were lysed in RIPA buffer (Cat. #20-188,
227 Millipore) containing protease inhibitor cocktail (Cat. # A32965, Thermo Scientific) on ice, followed by
228 brief sonication to prepare cell lysate. The BCA assay kit (Cat. #23225, Thermo Scientific) was used to
229 quantify the total protein amount in cell lysate, which was boiled in the SDS loading buffer with 5% β-

230 mercaptoethanol (Cat. #60-24-2, Acros Organics). The denatured protein samples were separated by
231 Novex™ WedgeWell™ 4-20% SDS-PAGE Tris-Glycine gel and transferred to PVDF membrane (iBlot™
232 2 Transfer Stacks, Invitrogen) using iBlot 2 Dry Blotting System (Cat. # IB21001, Thermo Scientific).
233 The membranes were blocked by 5% milk in PBST and probed by the specific primary antibodies at 4°C
234 overnight, followed by the HRP-conjugated secondary antibodies. The membranes were developed using
235 the Clarity Max ECL substrate (Cat. # 1705062, Bio-Rad).

236 **Luciferase reporter assays**

237 HEK293T cells were transfected with ISRE or NF-κB luciferase vector along with pRL-TK renilla
238 luciferase vector with or without the indicated vector expressing Nsp14. At 24 h post of transfection, the
239 medium was changed, and cells were treated with 10 ng/ml TNF-α or un-treated for 24h. Cells were lysed
240 using the Dual-Glo® Luciferase Assay System (Cat. #E2920, Promega). Luciferase/renilla signal intensity
241 was detected using Biotek Cytation5 and analyzed by GEN5 software (Biotek).

242 **Nuclear and cytoplasmic extraction**

243 HEK293T cells were transfected by pcDNA-FLAG-V5-Nsp14 or control vector pLex307-FLAG-V5
244 for 24h and changed fresh completed DMEM medium for further 24 h culture. Cells ($\sim 5 \times 10^6$ cells) were
245 collected, washed twice with 1× PBS, and subjected to the nucleus and cytoplasm extraction using NE-
246 PER Nuclear and Cytoplasmic Extraction Reagents (Cat. #78833, Thermo Scientific) following the
247 manufacturer's instructions and our previous studies (62). Total proteins in the whole-cell lysates from the
248 same number of cells were extracted using 1× RIPA buffer. Extractions from nuclear, cytoplasmic proteins
249 and the total cell lysate proteins were denatured and boiled with 4× LDS sample buffer (Cat. #NP0007,
250 Invitrogen) and subjected to immunoblotting analysis with equal protein loading of extracts ($\sim 20 \mu\text{g}/\text{lane}$).
251 Anti-GAPDH and anti-histone H3 immunoblotting were used as internal controls to determine the
252 cytoplasmic and nuclear fractions.

253 **Protein co-immunoprecipitation (co-IP)**

254 Protein co-IP assays were performed following the previously published protocol (62). Briefly, protein
255 A/G magnetic beads (Cat. # 88802, Thermo Scientific) and anti-FLAG M2 magnetic beads (Cat. # M8823,
256 Sigma-Aldrich) were washed with 1× RIPA buffer containing protease inhibitor cocktail. Cellular lysates
257 were precleared with the empty magnetic beads for 1 h at 4°C on a 360° tube rocker. The cell lysate was
258 incubated with anti-FLAG M2 magnetic beads for pull-down of FLAG-Nsp14 protein at 4°C overnight
259 with constant rotation. Protein immunocomplexes were washed by RIPA buffer and boiled in SDS loading
260 buffer containing 5% 2-mercaptoethanol, followed by protein immunoblotting. A normal mouse IgG
261 antibody (Cat. # sc-2025, Santa Cruz) was used as the control in parallel.

262 **Quantitative reverse transcription PCR (RT-qPCR)**

263 RT-qPCR assays were performed following the previously published protocol (64). Total RNAs
264 from harvested cells were extracted using the NucleoSpin RNA extraction kit (Cat. # 740955.250,
265 MACHEREY-NAGEL), and 0.4-1 µg RNA was reversely transcribed using the iScript™ cDNA
266 Synthesis Kit (Cat. # 1708890, Bio-Rad). Real-time qPCR was conducted using the iTaq™ Universal
267 SYBR® GreenSupermix (Cat. # 1727125, Bio-Rad). The PCR reaction was performed on a Bio-Rad
268 CFX connect qPCR machine under the following conditions: 95 °C for 10 m, 50 cycles of 95 °C for 15
269 s, and 60 °C for 1 m. Relative gene expression was normalized to GAPDH internal control as the $2^{-\Delta\Delta Ct}$
270 method: $2^{(\Delta Ct \text{ of targeted gene} - \Delta Ct \text{ of GAPDH})}$. The following primers were used. IL-4 forward: 5'-
271 GTTCTACAGCCACCATGAGAA-3', reverse: 5'-CCGTTTCAGGAATCAGATCA-3'; IL-6 forward:
272 5'-ACTCACCTCTTCAGAACGAATTG-3', reverse: 5'-CCATCTTTGGAAGGTTTCAGGTTG-3'(30);
273 IL-8 forward: 5'-CTTGGCAGCCTTCCTGATTT-3'; reverse: 5'-GGGTGGAAAGGTTTGGAGTATG-
274 3'; Nsp14 forward: 5'-CGGAAACCCAAAGGCTATCA-3', reverse: 5'-
275 TGTGGGTAGCGTAAGAGTAGAA-3'; IMPDH2 forward: 5'-CTCCCTGGGTACATCGACTT-3',

276 reverse: 5'-GCCTCTGTGACTGTGTCCAT-3'(64); GAPDH forward: 5'-
277 GCCTCTTGTCTCTTAGATTTGGTC-3', reverse: 5'-TAGCACTCACCATGTAGTTGAGGT-3'.
278 SARS-CoV-2-TRS-L (N sgRNA forward): CTCTTGATAGATCTGTTCTCTAAACGAAC,
279 SARS-CoV-2-TRS-N (N sgRNA reverse):GGTCCACCAAACGTAATGCG(65)

280 **Viral infection**

281 SARS-CoV-2 strain USA-WA1/2020 was obtained from BEI Resources, NIH, NIAHD (Cat #
282 NR52281) and was plaque purified in Vero E6 cells to identify plaques lacking furin cleavage site
283 mutations. A WT virus plaque was then propagated on Vero E6 cells stably expressing TMPRSS2 (kindly
284 provided by Dr. Shan-Lu Liu, Ohio State University) for 72 h. The virus was aliquoted, flash-frozen in
285 liquid nitrogen, and stored at -80C. The virus stock was titered on Vero E6 cells by TCID50 assay. For
286 infection experiments, the virus was added to cells for 24 h. Cells were then collected by trypsinization
287 and were either lysed with Trizol reagent for RNA extraction or were fixed with 4% paraformaldehyde in
288 PBS for 1 h prior to staining for flow cytometry. Staining was performed with anti-SARS-CoV-2 N (Cat
289 # 40143-MM08, Sino Biological) as described previously (28, 66). Flow cytometry was performed on a
290 FACSCanto II machine (BD Biosciences). Data were analyzed using FlowJo software.

291 **Human subjects**

292 The lung specimens from deceased COVID-19 patients were obtained from Biobank at Columbia
293 University Irving Medical Center. The control normal lung specimens were the gifts from Jahar
294 Bhattacharya (Columbia University, NY, USA). For paraffin sections, The lungs were fixed with 4%
295 paraformaldehyde (PFA) at 4°C overnight, dehydrated through a series of grade ethanol, and incubated
296 with Histo-Clear (Cat.5989-27-5, National Diagnostics, USA) at room temperature for 2 hours prior to
297 paraffin embedding. 7 µm thick sections were then prepared from the paraffin blocks and mounted on the
298 slides for staining.

299 **Protein immunofluorescence**

300 Paraffin-embedded lung tissue blocks were baked on the hotplate at 75 °C for 20 min and
301 deparaffinized in xylene. The slides were rehydrated from 100%, 90%, to 70% alcohol, and then to PBS.
302 We performed the antigen unmasking using the retriever (Cat. # 62700-10, Electron Microscopy Sciences)
303 with R-Buffer A pH 6.0 (Cat. # 62706-10, Electron Microscopy Sciences) for 2 h to complete the cycle
304 and cool down. Slides were blocked with 20% normal goat serum (NGS) in PBST for 2 h at room
305 temperature. Slides were incubated with an anti-IL-8 antibody (Cat. # 550419, BD Pharmingen™) in 5%
306 NGS with PBS at 4°C for overnight. Slides were washed with PBST and incubated with Alexa 488 coated
307 goat anti-mouse antibody in 5% NGS/PBS for 2 h at room temperature. Slides were washed with PBST
308 and stained with Hoechst (1:5000 in PBS, Invitrogen). Coverslips were mounted on slides using ProLong
309 Glass Antifade Mountant (Cat. # P36982, Invitrogen) and dried out in the dark overnight. Confocal images
310 were acquired using the ZEISS LSM 700 Upright laser scanning confocal microscope and ZEN imaging
311 software (ZEISS).

312 **Statistics**

313 Statistical analysis was performed using the GraphPad PRISM. Data are presented as mean \pm SD of
314 biological repeats from at least 2 independent experiments. * $p < 0.05$, ** $p < 0.01$, *** $p < 0.001$, or ****
315 $p < 0.001$ indicated the significant difference analyzed by ANOVA or Student's t-test.

316

317 **Acknowledgments**

318 The authors thank Dr. Mark Peeples (Nationwide Children's Hospital) and Dr. Jianrong Li (The Ohio
319 State University) for kindly providing plaque purified SARS-CoV-2 for viral propagation. We thank Dr.
320 Sheng-Ce Tao (Shanghai Jiao Tong University) for providing Nsp14 cloning plasmid. We also thank Dr.
321 Karin Musier-Forsyth and Dr. Shan-Lu Liu at The Ohio State University for their advice on our studies.

322 This study was funded by NIH research grants R01AI150448, R01DE025447, and R33AI116180 to J.Z.,
323 and R03DE029716, R01CA260690 to N.S.

324

325

326

327

328

329

330

331

332

333

334

335

336

337

338

339

340

341

342

343

344

345 References

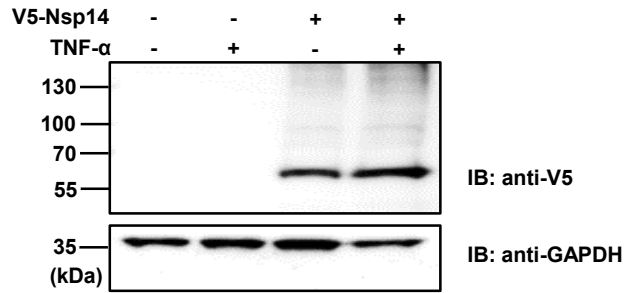
- 346 1. F. Robson *et al.*, Coronavirus RNA Proofreading: Molecular Basis and Therapeutic Targeting.
347 *Mol Cell* **80**, 1136-1138 (2020).
- 348 2. A. A. Naqvi *et al.*, Insights into SARS-CoV-2 genome, structure, evolution, pathogenesis and
349 therapies: Structural genomics approach. *Bba-Mol Basis Dis* **1866**, (2020).
- 350 3. X. Lei *et al.*, Activation and evasion of type I interferon responses by SARS-CoV-2. *Nat*
351 *Commun* **11**, 3810 (2020).
- 352 4. C. K. Yuen *et al.*, SARS-CoV-2 nsp13, nsp14, nsp15 and orf6 function as potent interferon
353 antagonists. *Emerg Microbes Infect* **9**, 1418-1428 (2020).
- 354 5. D. Blanco-Melo *et al.*, Imbalanced Host Response to SARS-CoV-2 Drives Development of
355 COVID-19. *Cell* **181**, 1036-1045 e1039 (2020).
- 356 6. M. Sa Ribero, N. Jouvenet, M. Dreux, S. Nisole, Interplay between SARS-CoV-2 and the type I
357 interferon response. *PLoS Pathog* **16**, e1008737 (2020).
- 358 7. M. Aid *et al.*, Vascular Disease and Thrombosis in SARS-CoV-2-Infected Rhesus Macaques.
359 *Cell* **183**, 1354-1366 e1313 (2020).
- 360 8. J. S. Y. Ho *et al.*, TOP1 inhibition therapy protects against SARS-CoV-2-induced lethal
361 inflammation. *Cell*, (2021).
- 362 9. Y. Ma *et al.*, Structural basis and functional analysis of the SARS coronavirus nsp14-nsp10
363 complex. *Proc Natl Acad Sci U S A* **112**, 9436-9441 (2015).
- 364 10. F. Ferron *et al.*, Structural and molecular basis of mismatch correction and ribavirin excision
365 from coronavirus RNA. *Proc Natl Acad Sci U S A* **115**, E162-E171 (2018).
- 366 11. E. Minskaia *et al.*, Discovery of an RNA virus 3'->5' exoribonuclease that is critically involved
367 in coronavirus RNA synthesis. *Proc Natl Acad Sci U S A* **103**, 5108-5113 (2006).
- 368 12. M. Bouvet *et al.*, RNA 3'-end mismatch excision by the severe acute respiratory syndrome
369 coronavirus nonstructural protein nsp10/nsp14 exoribonuclease complex. *Proc Natl Acad Sci U S*
370 *A* **109**, 9372-9377 (2012).
- 371 13. N. S. Ogando *et al.*, The Enzymatic Activity of the nsp14 Exoribonuclease Is Critical for
372 Replication of MERS-CoV and SARS-CoV-2. *J Virol* **94**, (2020).
- 373 14. N. H. Moeller *et al.*, Structure and dynamics of SARS-CoV-2 proofreading exoribonuclease
374 ExoN. *bioRxiv*, (2021).
- 375 15. Y. Chen *et al.*, Functional screen reveals SARS coronavirus nonstructural protein nsp14 as a
376 novel cap N7 methyltransferase. *Proc Natl Acad Sci U S A* **106**, 3484-3489 (2009).
- 377 16. M. Bouvet *et al.*, In vitro reconstitution of SARS-coronavirus mRNA cap methylation. *PLoS*
378 *Pathog* **6**, e1000863 (2010).
- 379 17. Y. Chen *et al.*, Biochemical and structural insights into the mechanisms of SARS coronavirus
380 RNA ribose 2'-O-methylation by nsp16/nsp10 protein complex. *PLoS Pathog* **7**, e1002294
381 (2011).
- 382 18. E. Decroly, F. Ferron, J. Lescar, B. Canard, Conventional and unconventional mechanisms for
383 capping viral mRNA. *Nat Rev Microbiol* **10**, 51-65 (2011).
- 384 19. Z. A. Jaafar, J. S. Kieft, Viral RNA structure-based strategies to manipulate translation. *Nat Rev*
385 *Microbiol* **17**, 110-123 (2019).
- 386 20. E. Jan, I. Mohr, D. Walsh, A Cap-to-Tail Guide to mRNA Translation Strategies in Virus-
387 Infected Cells. *Annu Rev Virol* **3**, 283-307 (2016).
- 388 21. M. Becares *et al.*, Mutagenesis of Coronavirus nsp14 Reveals Its Potential Role in Modulation of
389 the Innate Immune Response. *J Virol* **90**, 5399-5414 (2016).

- 390 22. J. Gribble *et al.*, The coronavirus proofreading exoribonuclease mediates extensive viral
391 recombination. *PLoS Pathog* **17**, e1009226 (2021).
- 392 23. D. E. Gordon *et al.*, A SARS-CoV-2 protein interaction map reveals targets for drug
393 repurposing. *Nature* **583**, 459-468 (2020).
- 394 24. L. X. Liao *et al.*, Highly selective inhibition of IMPDH2 provides the basis of
395 antineuroinflammation therapy. *Proc Natl Acad Sci U S A* **114**, E5986-E5994 (2017).
- 396 25. T. Liu, L. Zhang, D. Joo, S. C. Sun, NF-kappaB signaling in inflammation. *Signal Transduct*
397 *Target Ther* **2**, (2017).
- 398 26. C. Grassl, B. Luckow, D. Schlondorff, U. Dendorfer, Transcriptional regulation of the
399 interleukin-6 gene in mesangial cells. *J Am Soc Nephrol* **10**, 1466-1477 (1999).
- 400 27. V. Bezzerri *et al.*, Mapping the transcriptional machinery of the IL-8 gene in human bronchial
401 epithelial cells. *J Immunol* **187**, 6069-6081 (2011).
- 402 28. G. Shi *et al.*, Opposing activities of IFITM proteins in SARS-CoV-2 infection. *Embo J* **40**,
403 e106501 (2021).
- 404 29. L. Leng *et al.*, Pathological features of COVID-19-associated lung injury: a preliminary
405 proteomics report based on clinical samples. *Signal Transduct Target Ther* **5**, 240 (2020).
- 406 30. J. C. Melms *et al.*, A molecular single-cell lung atlas of lethal COVID-19. *Nature*, (2021).
- 407 31. L. Hedstrom, IMP dehydrogenase: structure, mechanism, and inhibition. *Chem Rev* **109**, 2903-
408 2928 (2009).
- 409 32. S. Zhou, R. Liu, B. M. Baroudy, B. A. Malcolm, G. R. Reyes, The effect of ribavirin and
410 IMPDH inhibitors on hepatitis C virus subgenomic replicon RNA. *Virology* **310**, 333-342
411 (2003).
- 412 33. P. Leysen, J. Balzarini, E. De Clercq, J. Neyts, The predominant mechanism by which ribavirin
413 exerts its antiviral activity in vitro against flaviviruses and paramyxoviruses is mediated by
414 inhibition of IMP dehydrogenase. *J Virol* **79**, 1943-1947 (2005).
- 415 34. M. D. Sintchak *et al.*, Structure and mechanism of inosine monophosphate dehydrogenase in
416 complex with the immunosuppressant mycophenolic acid. *Cell* **85**, 921-930 (1996).
- 417 35. C. W. Yang *et al.*, Targeting Coronaviral Replication and Cellular JAK2 Mediated Dominant
418 NF-kappaB Activation for Comprehensive and Ultimate Inhibition of Coronaviral Activity. *Sci*
419 *Rep* **7**, 4105 (2017).
- 420 36. N. Hemmat *et al.*, The roles of signaling pathways in SARS-CoV-2 infection; lessons learned
421 from SARS-CoV and MERS-CoV. *Arch Virol* **166**, 675-696 (2021).
- 422 37. X. Yin *et al.*, MDA5 Governs the Innate Immune Response to SARS-CoV-2 in Lung Epithelial
423 Cells. *Cell Rep* **34**, 108628 (2021).
- 424 38. M. M. Rahman, G. McFadden, Modulation of NF-kappaB signalling by microbial pathogens.
425 *Nat Rev Microbiol* **9**, 291-306 (2011).
- 426 39. J. L. Forbester, I. R. Humphreys, Genetic influences on viral-induced cytokine responses in the
427 lung. *Mucosal Immunol* **14**, 14-25 (2021).
- 428 40. R. Alon *et al.*, Leukocyte trafficking to the lungs and beyond: lessons from influenza for
429 COVID-19. *Nat Rev Immunol* **21**, 49-64 (2021).
- 430 41. C. M. Ziegler *et al.*, A Proteomics Survey of Junin Virus Interactions with Human Proteins
431 Reveals Host Factors Required for Arenavirus Replication. *J Virol* **92**, (2018).
- 432 42. W. Dang *et al.*, Inhibition of Calcineurin or IMP Dehydrogenase Exerts Moderate to Potent
433 Antiviral Activity against Norovirus Replication. *Antimicrob Agents Chemother* **61**, (2017).
- 434 43. W. P. Hofmann, E. Herrmann, C. Sarrazin, S. Zeuzem, Ribavirin mode of action in chronic
435 hepatitis C: from clinical use back to molecular mechanisms. *Liver Int* **28**, 1332-1343 (2008).

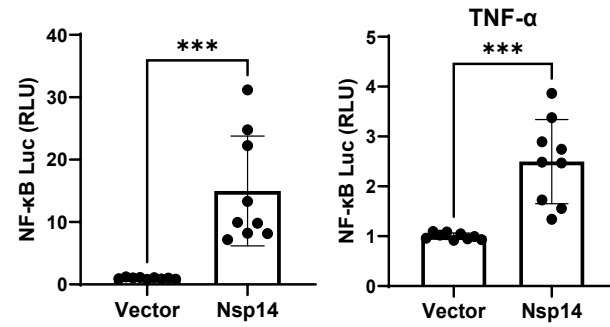
- 436 44. L. Quemeneur *et al.*, Differential control of cell cycle, proliferation, and survival of primary T
437 lymphocytes by purine and pyrimidine nucleotides. *J Immunol* **170**, 4986-4995 (2003).
- 438 45. Q. N. Shu, V. Nair, Inosine monophosphate dehydrogenase (IMPDH) as a target in drug
439 discovery. *Med Res Rev* **28**, 219-232 (2008).
- 440 46. J. Toubiana *et al.*, IMPDHII protein inhibits Toll-like receptor 2-mediated activation of NF-
441 kappaB. *J Biol Chem* **286**, 23319-23333 (2011).
- 442 47. S. Kofuji *et al.*, IMP dehydrogenase-2 drives aberrant nucleolar activity and promotes
443 tumorigenesis in glioblastoma. *Nat Cell Biol* **21**, 1003-1014 (2019).
- 444 48. S. Kofuji, A. T. Sasaki, GTP metabolic reprogramming by IMPDH2: unlocking cancer cells'
445 fuelling mechanism. *J Biochem* **168**, 319-328 (2020).
- 446 49. Q. Zhang *et al.*, The role of IMP dehydrogenase 2 in Inauhzin-induced ribosomal stress. *Elife* **3**,
447 (2014).
- 448 50. S. Mannava *et al.*, Direct role of nucleotide metabolism in C-MYC-dependent proliferation of
449 melanoma cells. *Cell Cycle* **7**, 2392-2400 (2008).
- 450 51. J. Zhang *et al.*, A systemic and molecular study of subcellular localization of SARS-CoV-2
451 proteins. *Signal Transduct Target Ther* **5**, 269 (2020).
- 452 52. J. M. Meyers *et al.*, The proximal proteome of 17 SARS-CoV-2 proteins links to disrupted
453 antiviral signaling and host translation. *bioRxiv*, (2021).
- 454 53. B. R. Lane *et al.*, Interleukin-8 stimulates human immunodeficiency virus type 1 replication and
455 is a potential new target for antiretroviral therapy. *J Virol* **75**, 8195-8202 (2001).
- 456 54. W. C. Chen *et al.*, HCV NS5A Up-Regulates COX-2 Expression via IL-8-Mediated Activation
457 of the ERK/JNK MAPK Pathway. *Plos One* **10**, e0133264 (2015).
- 458 55. N. Mukaida, Pathophysiological roles of interleukin-8/CXCL8 in pulmonary diseases. *Am J*
459 *Physiol Lung Cell Mol Physiol* **284**, L566-577 (2003).
- 460 56. T. Murayama *et al.*, Enhancement human cytomegalovirus replication in a human lung fibroblast
461 cell line by interleukin-8. *J Virol* **68**, 7582-7585 (1994).
- 462 57. J. Hiscott, H. Kwon, P. Genin, Hostile takeovers: viral appropriation of the NF-kappaB pathway.
463 *J Clin Invest* **107**, 143-151 (2001).
- 464 58. I. F. Hung *et al.*, Triple combination of interferon beta-1b, lopinavir-ritonavir, and ribavirin in
465 the treatment of patients admitted to hospital with COVID-19: an open-label, randomised, phase
466 2 trial. *Lancet* **395**, 1695-1704 (2020).
- 467 59. W. Wan *et al.*, High-Throughput Screening of an FDA-Approved Drug Library Identifies
468 Inhibitors against Arenaviruses and SARS-CoV-2. *ACS Infect Dis*, (2020).
- 469 60. Y. Han *et al.*, Identification of SARS-CoV-2 inhibitors using lung and colonic organoids. *Nature*
470 **589**, 270-275 (2021).
- 471 61. E. Prinarakis, E. Chantzoura, D. Thanos, G. Spyrou, S-glutathionylation of IRF3 regulates IRF3-
472 CBP interaction and activation of the IFN beta pathway. *Embo J* **27**, 865-875 (2008).
- 473 62. D. Zhou *et al.*, Inhibition of Polo-like kinase 1 (PLK1) facilitates the elimination of HIV-1 viral
474 reservoirs in CD4(+) T cells ex vivo. *Sci Adv* **6**, eaba1941 (2020).
- 475 63. W. Kong *et al.*, Nucleolar protein NOP2/NSUN1 suppresses HIV-1 transcription and promotes
476 viral latency by competing with Tat for TAR binding and methylation. *PLoS Pathog* **16**,
477 e1008430 (2020).
- 478 64. F. Huang *et al.*, Inosine Monophosphate Dehydrogenase Dependence in a Subset of Small Cell
479 Lung Cancers. *Cell Metab* **28**, 369-382 e365 (2018).

- 480 65. L. Yang *et al.*, A Human Pluripotent Stem Cell-based Platform to Study SARS-CoV-2 Tropism
481 and Model Virus Infection in Human Cells and Organoids. *Cell Stem Cell* **27**, 125-136 e127
482 (2020).
- 483 66. R. C. Larue *et al.*, Rationally Designed ACE2-Derived Peptides Inhibit SARS-CoV-2. *Bioconjug*
484 *Chem* **32**, 215-223 (2021).
- 485

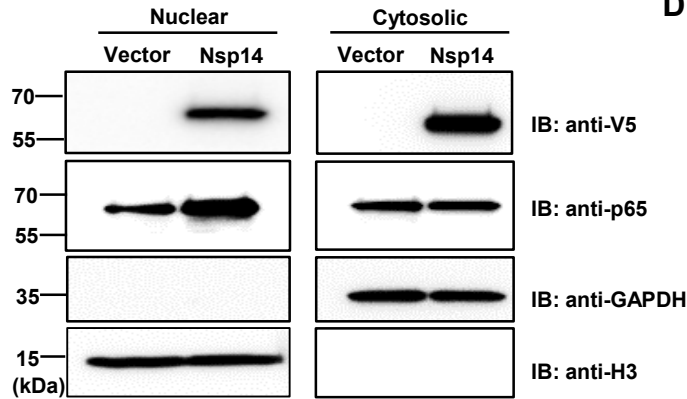
A



B



C



D

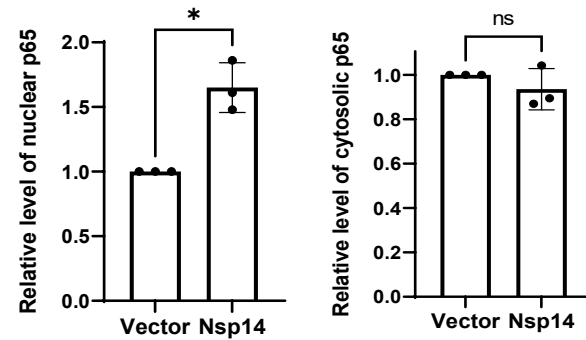


Fig 1. SARS-CoV-2 Nsp14 increases NF- κ B activity. (A-C) HEK293T cells were transiently transfected with V5-FLAG-Nsp14 or empty vector, and treated with or without TNF- α . V5-FLAG-Nsp14 was analyzed by protein immunoblotting (**A**). HEK293T cells transfected with V5-FLAG-Nsp14 or empty vector along with NF- κ B-driven firefly luciferase and TK-driven renilla luciferase reporter vectors were un-treated or treated with TNF- α (**B**). Luciferase activity (firefly/renilla) in these cells was measured and normalized to the empty vector. HEK293T cells transfected with V5-FLAG-Nsp14 or empty vector were subjected to the nuclear/cytosolic fractionation. V5-FLAG-Nsp14 and NF- κ B p65 in the nucleus or cytosol were analyzed by protein immunoblotting (**C**). Histone H3 was used as the nuclear marker. The intensity of the p65 protein band was quantified and normalized to the empty vector (**D**). Results were calculated from 3 independent experiments and presented as mean +/- standard deviation (SD). (* $p < 0.05$; *** $p < 0.001$ by unpaired Student's t-test).

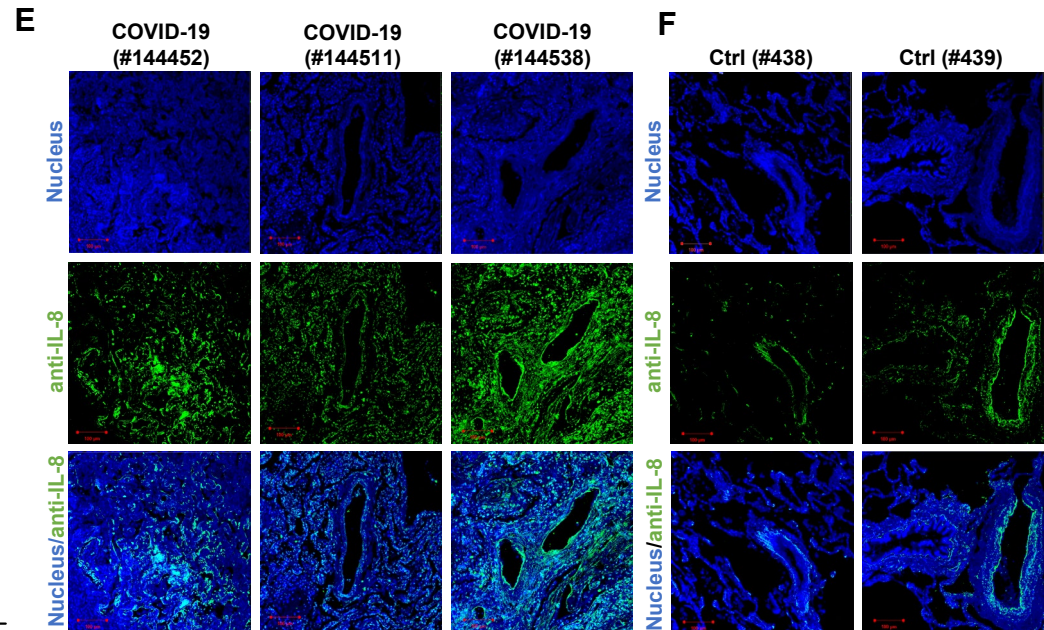
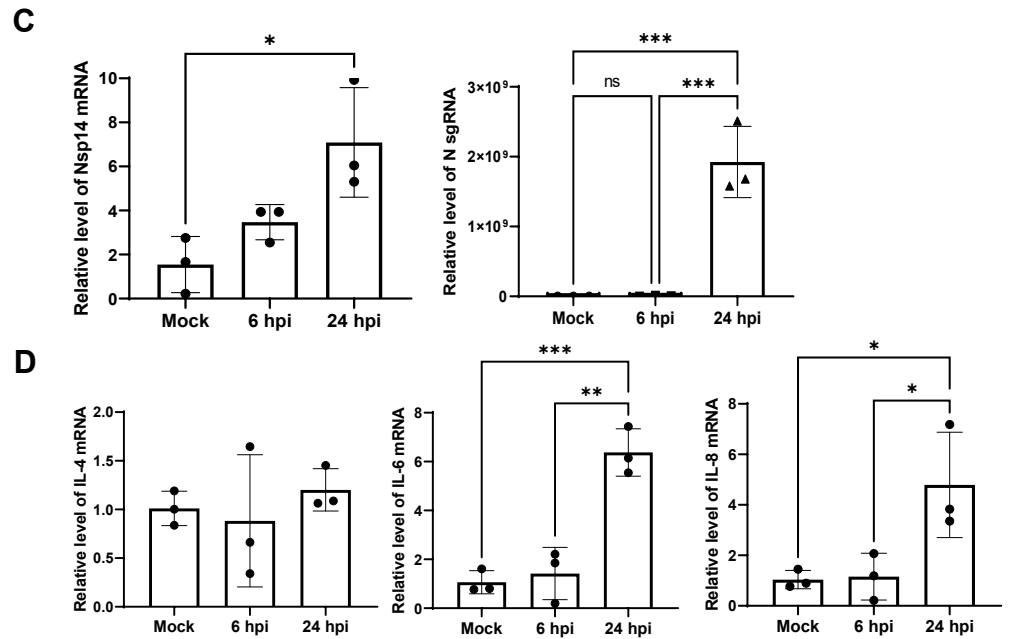
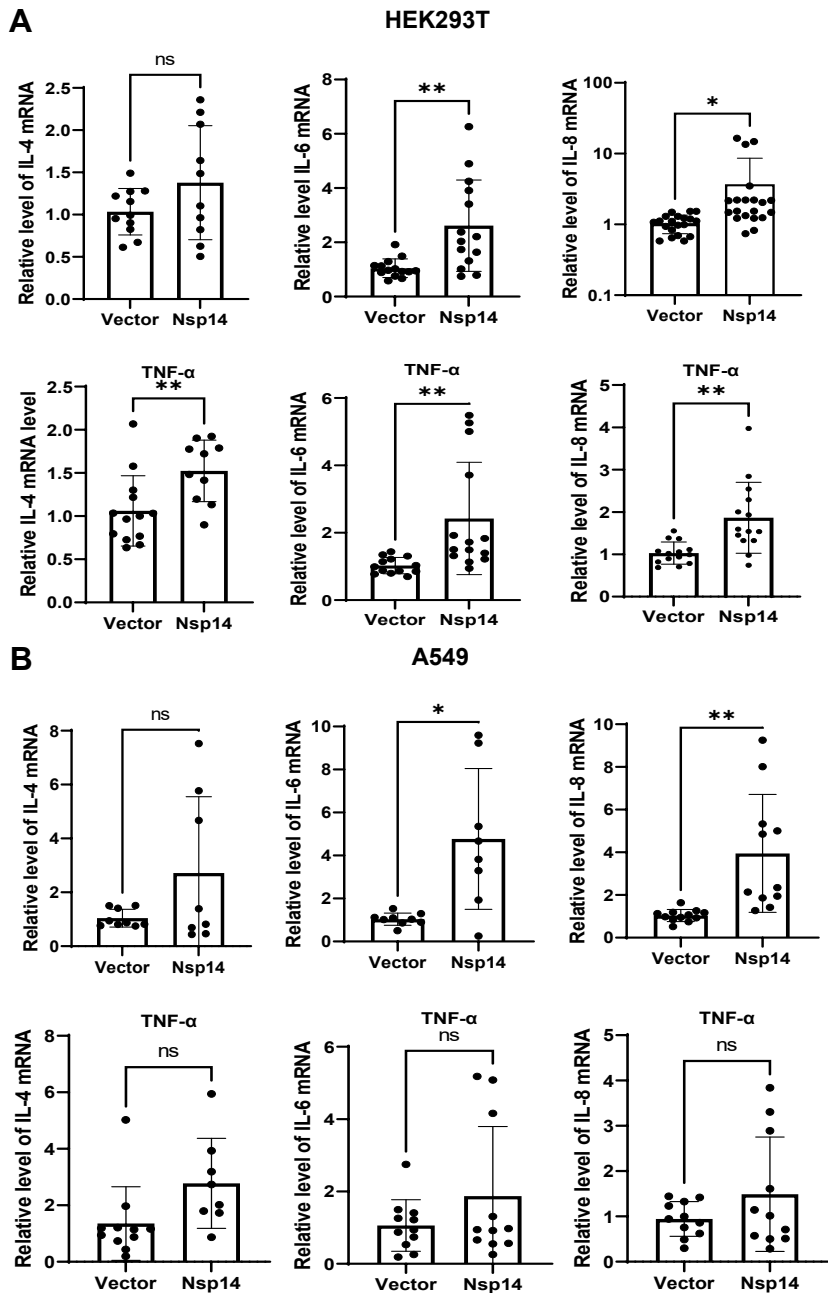


Fig 2. SARS-CoV-2 Nsp14 increases IL-6/8 expression. (A) HEK293T cells were transfected with V5-FLAG-Nsp14 or empty vector were un-treated or treated with TNF- α . The mRNA level of IL-4/6/8 in these cells was measured and normalized to the empty vector. (B) A549 cells were treated similarly as in (A) and analyzed for IL-4/6/8 expression. Results were calculated from at least 3 independent experiments and presented as mean +/- standard deviation (SD). (* p <0.05; ** p <0.01; by unpaired Student's t-test). (C, D) HEK293T-ACE2 cells were infected with wild-type SARS-Cov-2 viruses. Cells were harvested at the indicated time points. Total RNAs were extracted, and expression of viral genes (Nsp14, N-protein, C) or ILs (IL-4, 6, 8, D) was analyzed by RT-qPCR and normalized to mock infection. Results were calculated from 3 technical repeats and presented as mean +/- standard deviation (SD). (* p <0.05; ** p <0.01; *** p <0.001 by one-way ANOVA and Tukey's multiple comparison test). (E, F) Dissected lung tissues from COVID19 patients (E, donors #144452, #144511, #144538) or non-infected donors (F, donors #438, #439) were analyzed for IL-8 expression by immunofluorescence (green). Nuclei were stained with Hoechst (blue). Scale bar: 100 μ m.

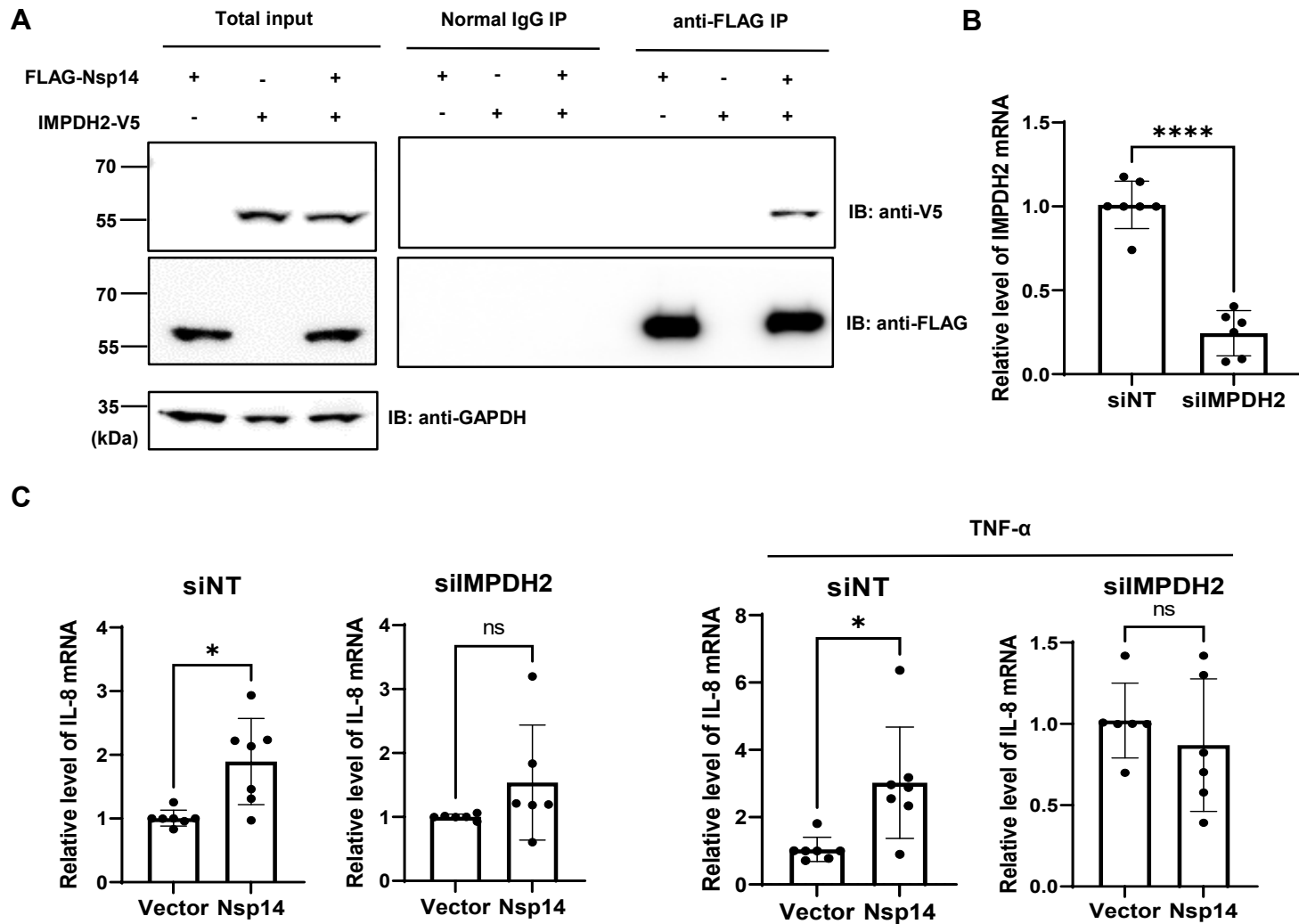


Fig 3. IMPDH2 associates with Nsp14 and is required for IL-8 upregulation by Nsp14. (A) HEK293T cells were transiently transfected with the vector expressing FLAG-Nsp14 or V5-IMPDH2, alone or together. Cell lysates were prepared and subjected to protein co-immunoprecipitation (co-IP) assays using anti-FLAG or control IgG antibody. Precipitated protein samples were analyzed by protein immunoblotting using anti-V5 and anti-FLAG antibodies. (B) HEK293T cells were transiently transfected with IMPDH2 or non-targeting (NT) siRNAs. mRNA level of IMPDH2 was measured and normalized to siNT. (C) HEK293T cells transfected with IMPDH2 or NT siRNAs were further transfected with V5-FLAG-Nsp14 or empty vector. These cells were untreated or treated with TNF- α . Total RNAs were extracted. IL-8 mRNA was analyzed and normalized to the empty vector. Results were calculated from 3 independent experiments and presented as mean \pm standard deviation (SD). (* $p < 0.05$; **** $p < 0.0001$ by unpaired Student's t-test).

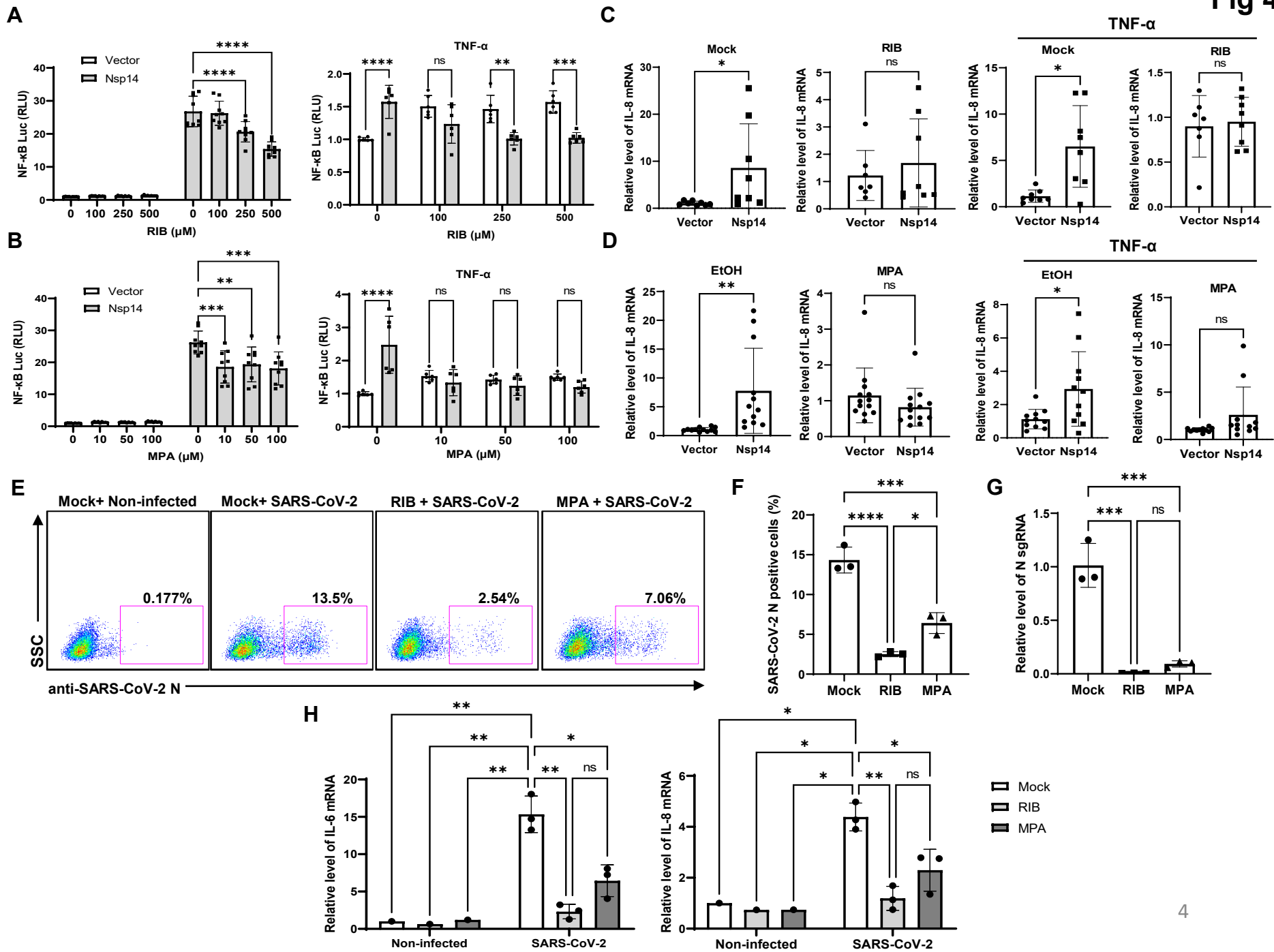


Fig 4. IMPDH2 inhibition reduces Nsp14-mediated NF- κ B activation and IL8 induction. (A)

HEK293T cells transfected with V5-FLAG-Nsp14 or empty vector along with NF- κ B-driven firefly luciferase and TK-driven renilla luciferase reporter vectors were treated with ribavirin (RIB) at the basal or TNF α -stimulated condition. Luciferase activity (firefly/renilla) in these cells was measured and normalized to that of un-treated, empty vector-transfected cells. **(B)** Mycophenolic acid (MPA) was tested similarly as in **(A)**. Results were calculated from at least 2 independent experiments and presented as mean \pm standard deviation (SD). (** $p < 0.01$; *** $p < 0.001$; **** $p < 0.0001$ by two-way ANOVA and Tukey's multiple comparison test). **(C)** HEK293T cells transfected with V5-FLAG-Nsp14 or empty vector were treated with RIB at the basal or TNF- α -stimulated condition. Total RNAs were extracted. IL-8 mRNA was analyzed and normalized to the mock treatment. **(D)** MPA was tested similarly as in **(C)**, and results were normalized to the solvent control (0.1% ethanol, EtOH). Results were calculated from 3 independent experiments and presented as mean \pm standard deviation (SD). (* $p < 0.05$ by unpaired Student's t-test). **(E-H)** A549-ACE2 cells were treated with RIB (500 μ M), MPA (100 μ M), or mock, and infected with SARS-Cov-2 viruses for 24 h. The SARS-CoV-2 infection was detected by intracellular staining of SARS-CoV-2 N protein **(E)**. Percentage of SARS-CoV-2 N protein positive cells was calculated **(F)**. Cells were harvested for RNA extraction, and N protein sgRNA was analyzed and normalized to the mock treatment **(G)**. mRNA of IL-6 and IL-8 was analyzed and normalized to the non-infected cell with the mock treatment **(H)**. Results were calculated from 3 technical repeats and presented as mean \pm standard deviation (SD). (* $p < 0.05$; ** $p < 0.01$; *** $p < 0.001$; **** $p < 0.001$ by two-way ANOVA and Tukey's multiple comparison test).

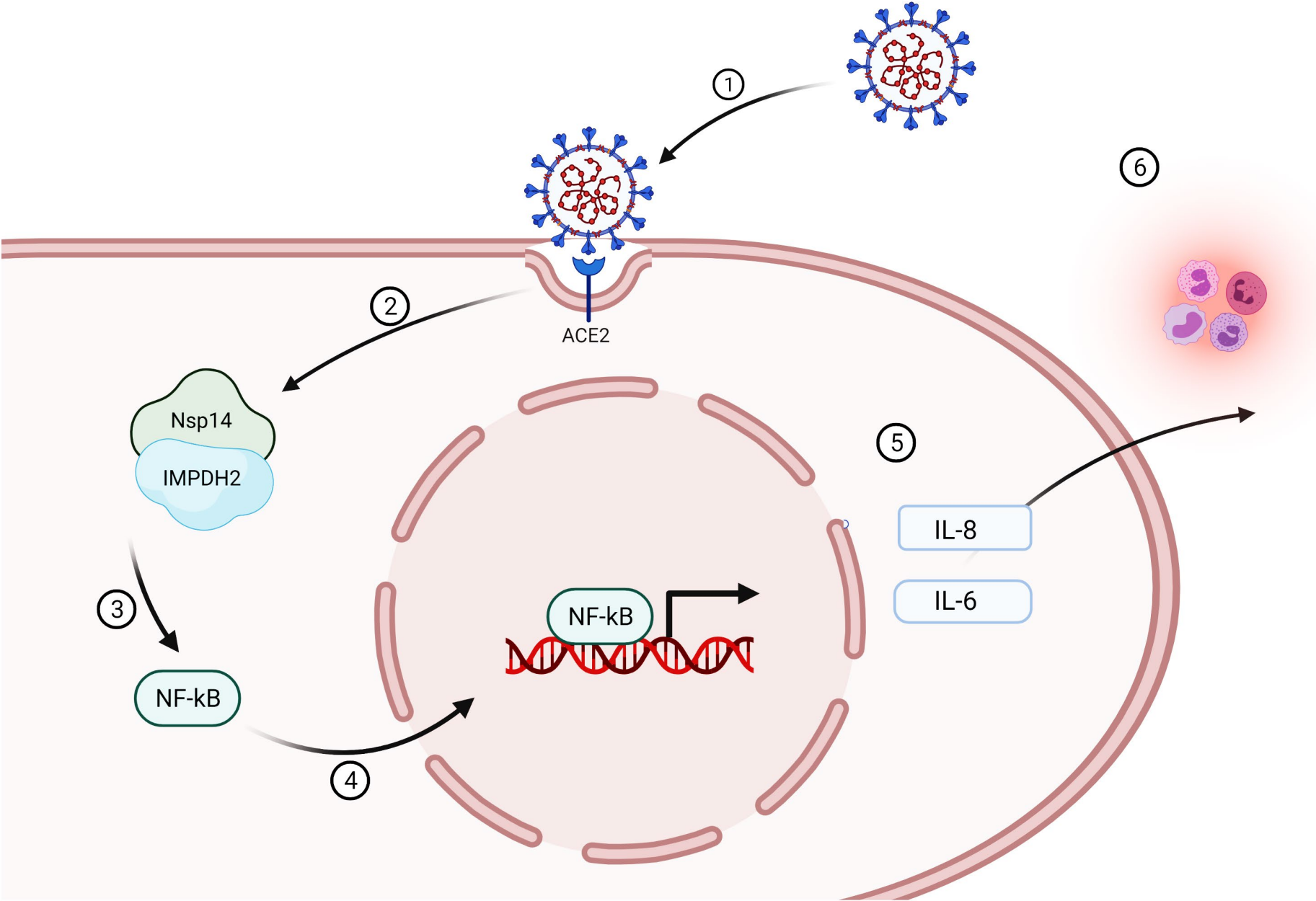


Fig 5. A working model of Nsp14-mediated NF- κ B activation in SARS-CoV-2 infection. Infection of SARS-CoV-2 (1) leads to the expression of Nsp14 (2) that interacts with IMPDH2 (3). Such interaction promotes the nuclear translocation of NF- κ B p65 (4) and its activation, which upregulates the expression of downstream cytokines, including IL-6 and IL-8 (5). Expression of IL-6 and IL-8 may further amplify the inflammatory response (6) and also in return benefit SARS-CoV-2 infection.

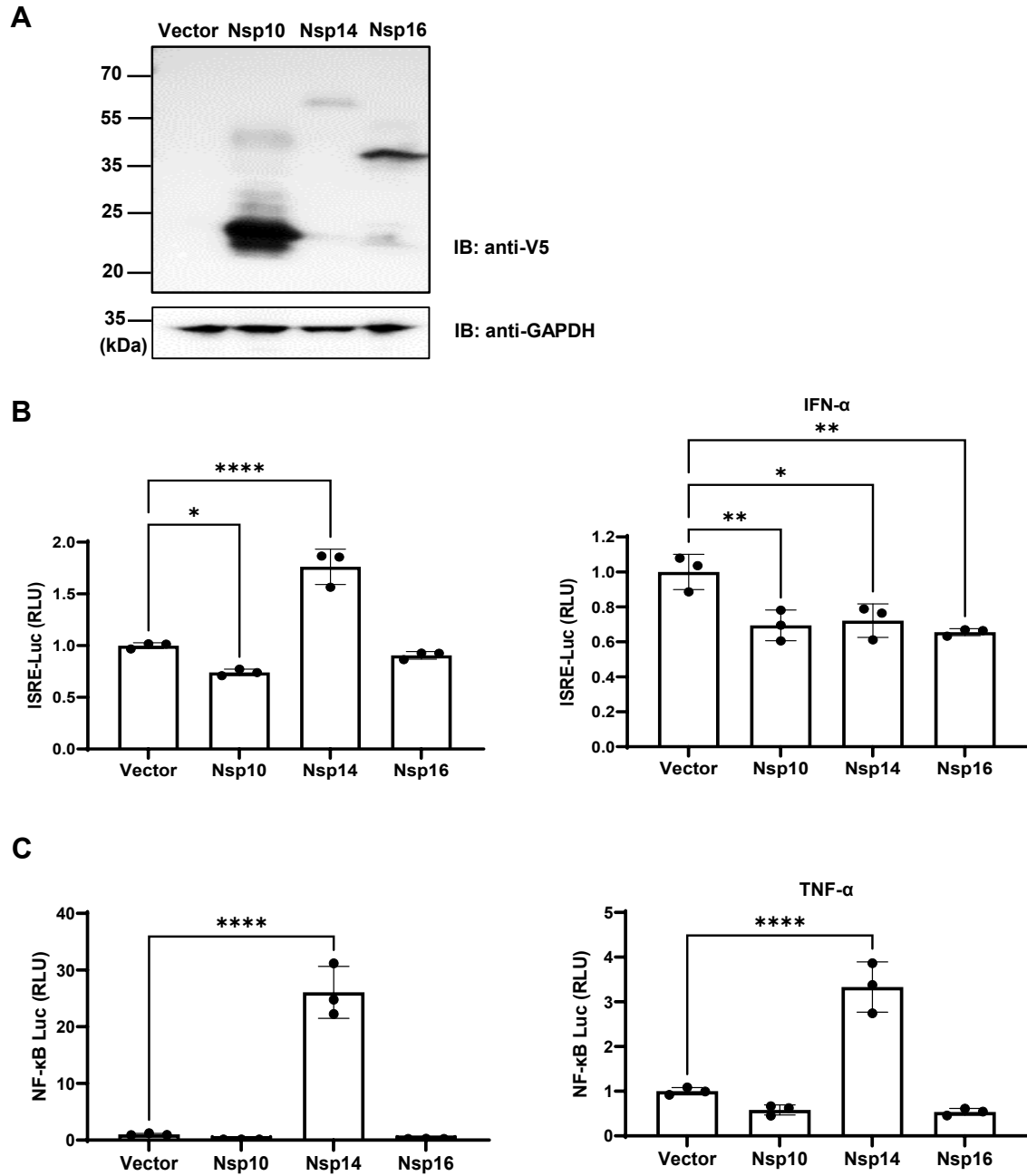


Fig S1. (A) HEK293T cells were transiently transfected with the vector expressing V5-FLAG-Nsp10, 14, 16, or empty vector. Protein expression was analyzed by protein immunoblotting. **(B)** HEK293T cells transfected with the vector expressing V5-FLAG-Nsp10, 14, 16, or empty vector along with ISRE-driven firefly luciferase and TK-driven renilla luciferase reporter vectors were un-treated or treated with IFN- α . **(C)** HEK293T cells transfected with the vector expressing V5-FLAG-Nsp10, 14, 16, or empty vector along with NF- κ B-driven firefly luciferase and TK-driven renilla luciferase reporter vectors were un-treated or treated with TNF- α . Luciferase activity (firefly/renilla) in these cells was measured and normalized to the empty vector. Results were calculated from 3 technical repeats and presented as mean +/- standard deviation (SD). (* p <0.05; ** p <0.01; *** p <0.001; **** p <0.0001 by unpaired Student's t-test).

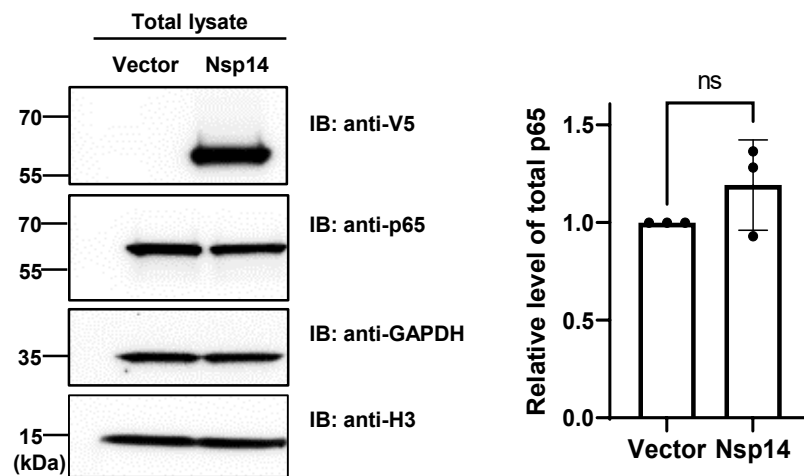


Fig S2. NF- κ B p65 in the total lysate of HEK293T cells transfected with the vector expressing V5-FLAG-Nsp14 or empty vector was analyzed by protein immunoblotting. Histone H3 was used as the nuclear marker. The intensity of the p65 protein band was quantified and normalized to the empty vector.

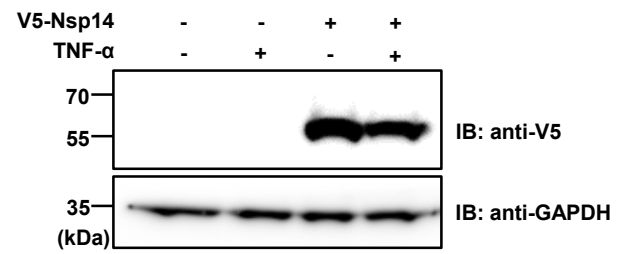
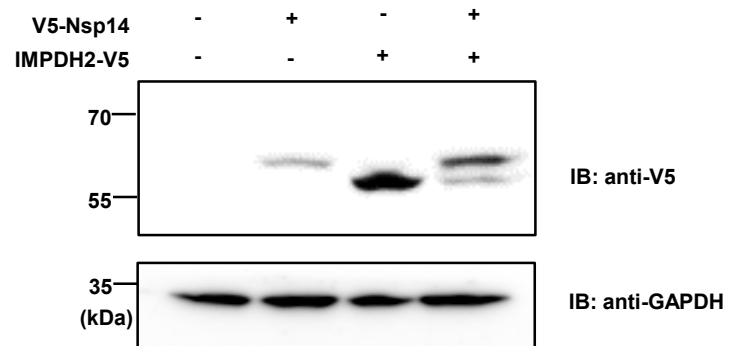


Fig S3. A549 cells were transiently transfected with the vector expressing V5-Nsp14 or empty vector, and treated with or without TNF α . V5-Nsp14 was analyzed by protein immunoblotting.

A



B

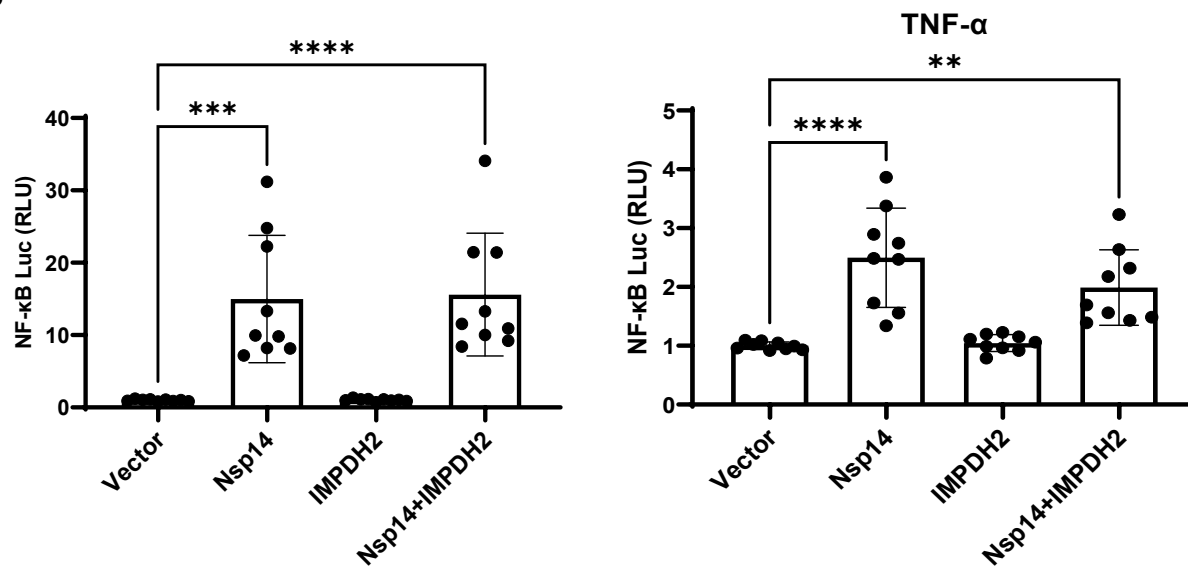
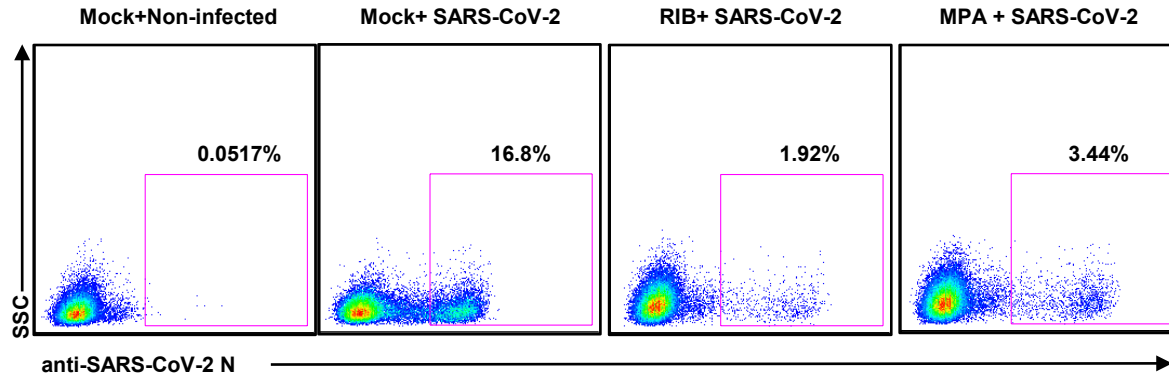
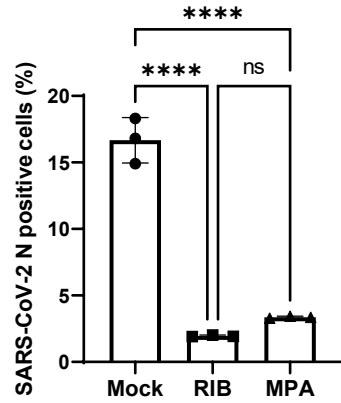


Fig S4. (A) HEK293T cells were transiently transfected with the vector expressing V5-Nsp14 or V5-IMP2, alone or together. Protein expression was analyzed by protein immunoblotting. (B) Cells in (A) further transfected with NF- κ B-driven firefly luciferase and TK-driven renilla luciferase reporter vectors were un-treated or treated with TNF- α . Luciferase activity (firefly/renilla) was measured and normalized to the empty vector. Results were calculated from 3 independent experiments and presented as mean \pm standard deviation (SD). (** $p < 0.01$; *** $p < 0.001$; **** $p < 0.0001$ by one-way ANOVA and Tukey's multiple comparison test)

A HEK293T-ACE2



B



C

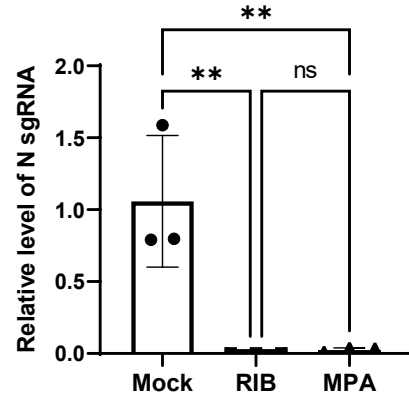


Fig S5. HEK293T-ACE2 cells were treated with RIB (500 μ M), or MPA (100 μ M), or mock, and infected with SARS-Cov-2 viruses for 24 h. The SARS-CoV-2 infection was detected by intracellular staining of SARS-CoV-2 N protein (**A**). Percentage of SARS-CoV-2 N protein positive cells was calculated (**B**). Cells were harvested for RNA extraction, and N protein sgRNA was analyzed and normalized to the mock treatment (**C**). The results were calculated from 3 technical repeats and presented as mean +/- standard deviation (SD). (** $p < 0.01$; **** $p < 0.001$ by one-way ANOVA and Tukey's multiple comparison test)